Available online at www.sciencedirect.com
ScienceDirect
Journal of Applied Geophysics 62 (2007) 124–140
JOURNAL OF APPLIED GEOPHYSICS
www.elsevier.com/locate/jappgeo

Combined weighted inversion of electrical resistivity data arising from different array types

E.N. Athanasiou *, P.I. Tsourlos, C.B. Papazachos, G.N. Tsokas

Applied Geophysics Laboratory, Aristotle University of Thessaloniki, 54124 Thessaloniki, Greece

Received 3 December 2004; accepted 4 September 2006

Abstract

In this work we examine the case of combined weighted inversion of resistivity data arising from different array types. In general, there is no single optimum array which can always give valid and useful results, independent of the target characteristics. Moreover, the geoelectrical models produced by the inversion of different arrays over the same structure can be different. In order to use all available information and produce a potentially more reliable geoelectrical model of the earth, an algorithm for the 2-D combined inversion of the most commonly used arrays (dipole–dipole, pole–dipole, Wenner–Schlumberger, Wenner) is examined. The use of this algorithm on several data sets showed that some arrays dominate over others. To overcome this problem an extra weighting factor is introduced to calibrate the participation of the data of each array into the inversion procedure. To determine the value of this factor we have used the Jacobian matrices which are computed for the data set of each array. The 2-D combined weighted inversion algorithm is tested with various synthetic data sets. Furthermore, a real field data application is presented. The results indicate that the algorithm provides an inverted model of all available data which is not necessarily the optimum but more effective when compared to just jointly inverting all data sets without weighting. The combined weighted inversion algorithm is proved to be a useful tool for data interpretation, especially when the area of study has complicate structures for which there is no *a priori* information and each array type can not solely produce a reliable geoelectrical model of the subsurface.

Keywords: Combined — joint weighted resistivity inversion; ERT; Resistivity arrays

1. Introduction

Over the last decade the Electrical Resistivity Tomography (ERT) has been extensively used in geophysical investigations (Dahlin, 2001). Compared to conventional measuring modes ERT prospecting can be successfully used in areas with complex geology, since it provides information in both lateral and vertical directions and defines in a qualitative manner the shape and depth of the subsurface targets. Resistivity acquisition instruments are used in order to carry out field measurements (Griffiths and Barker, 1993), while the interpretation of field or synthetic data is carried out by a number of inversion programs available (Loke and Barker, 1996a). Many geophysicists have shown that it is possible to reconstruct an accurate resistivity image of the subsurface using a large number of measured data and employing 2-D and 3-D imaging or inversion schemes (Li and Oldenburg, 1992; Loke and Barker, 1995, 1996a,b; LaBrecque et al., 1996).

During the last few years, there is a significant effort in ERT prospecting to develop techniques which obtain

* Corresponding author. Fax: +30 2310 998528.
E-mail address: athanael@geo.auth.gr (E.N. Athanasiou).

0926-9851/$ - see front matter © 2006 Elsevier B.V. All rights reserved.
doi:10.1016/j.jappgeo.2006.09.003

the maximum information from each data set and at the same time reduce the amount of data which need to be collected in the field. Dahlin and Zhou (2004) examined the surveying efficiency (anomaly effects, signal-to-noise ratios) and the imaging capabilities of ten electrode arrays over five synthetic geological models. They recommended the pole–dipole, dipole–dipole, Wenner–Schlumberger and gradient arrays for 2-D resistivity imaging.

However, the mapping of the study area with more than one array types, which have different theoretical and practical merits and demerits, can give different geoelectrical models. For example, Wenner and Wenner–Schlumberger arrays appear to have high vertical resolution, while dipole–dipole and pole–dipole arrays have high lateral resolution (Ward, 1989). Stummer et al. (2004) presented an experimental design procedure to identify non-conventional suites of electrode configurations that provide maximum subsurface information using a sensitivity based optimization scheme. They suggest that combined data sets coming from different configurations carry more information than the individual data sets.

In theory combined inversion of data sets coming from different electrode arrays obtained over the same site would allow us to combine the relative advantages of every array and thus to produce superior results. de la Vega et al. (2003) presented combined inversion results of dipole–dipole and Wenner array data obtained from a hydrocarbon contamination site. They suggested that combined inversion results have superior depth of investigation and better lateral resolution when compared to the inversion results obtained from each array separately.

However, the use of 2-D combined inversion algorithm on several data sets showed that some arrays dominate over others. For example, measurements obtained using the dipole–dipole array have typically twice stronger sensitivity than measurements obtained by the Wenner array. To overcome this problem a particular weighting factor can be applied to equalize the participation of the data of each array. Since the sensitivity (Jacobian) matrices associate variations in the model properties with variations in the observed data, the value of this factor uses the Jacobian matrices which are produced for the data set of each array. The present paper describes a 2-D combined weighted inversion algorithm based on a fully automated smoothness constrained 2-D inversion algorithm (Tsourlos, 1995).

The following section gives an outline of the mathematical formulations used by the 2-D combined weighted inversion algorithm. Moreover, results from several representative tests with synthetic and field data processed using the combined weighted inversion scheme are also presented.

2. Methodology

In the 2-D inversion algorithm, an optimally smooth geoelectrical model of the earth is calculated. This involves the inversion of the data until the roughness term dR is minimized under the constrain that the sum of squared errors S is also minimized or (since we are dealing with real data) becomes equal to X_{d}, which is the acceptable average error in view of data uncertainties. The values of dR and S are given by the equations:

$$\mathrm{d}R = (\mathbf{C}_x\mathrm{d}\mathbf{x})^T\mathbf{C}_x\mathrm{d}\mathbf{x} + (\mathbf{C}_z\mathrm{d}\mathbf{x})^T C_x\mathrm{d}\mathbf{x}, \tag{1}$$

$$S = (\mathbf{W}_{\mathrm{d}}\mathrm{d}\mathbf{y})^T(\mathbf{W}_{\mathrm{d}}\mathrm{d}\mathbf{y}), \tag{2}$$

where $\mathbf{C}x$, $\mathbf{C}z$ are model smoothness matrices in the x and z axes respectively (de Groot-Hedlin and Constable, 1990), d$\mathbf{y}$ is the vector of differences between the observed data $\mathbf{d}_{\mathrm{obs}}$ and the modeled data $\mathbf{d}_{\mathrm{calc}}$ (calculated using the forward modeling technique), $\mathbf{W}_{\mathrm{d}}$ is the data weighting matrix and T denotes the transpose. In the standard Bayesian formulation $\mathbf{W}_{\mathrm{d}}$ is the inverse square root of the *a priori* data covariance matrix, which is usually assumed (independent data errors) to be a diagonal matrix containing inverse data errors, σ_i, (i=1,...n) when using n data (e.g., Tarantola, 1984), in which case Eq. (2) becomes:

$$S = \sum_{i=1}^{n} \mathrm{d}y_i^2/\sigma_i^2 \tag{2a}$$

Minimization is achieved by the use of the Lagrangian multiplier technique, which yields the non-linear smoothness constrained inversion algorithm (Sasaki, 1992). The inversion is iterative and the resistivity $\mathbf{x}_{k+1}$ at the k+1th iteration is given by:

$$\begin{aligned}\mathbf{x}_{k+1} &= \mathbf{x}_k + \mathrm{d}\mathbf{x}_k = \mathbf{x}_k \\ &+ \left[(\mathbf{W}_{\mathrm{d}}\mathbf{J}_k)^T(\mathbf{W}_{\mathrm{d}}\mathbf{J}_k) + \mu_k(\mathbf{C}_x^T\mathbf{C}_x + \mathbf{C}_z^T\mathbf{C}_z)\right]^{-1} \\ &\times (\mathbf{W}_{\mathrm{d}}\mathbf{J}_k)^T\mathbf{W}_{\mathrm{d}}\mathrm{d}\mathbf{y}_k,\end{aligned} \tag{3}$$

where $\mathbf{J}_k$ and μ_k is the Jacobian matrix estimate and the Lagrangian multiplier respectively for the kth iteration. Note that in the above formulation it is common that logarithmic model resistivities and apparent resistivities

are used in order to constrain subsurface resistivity to be positive and to accelerate the convergence of the iterative algorithm (Park and Van, 1991).

Inversion's theoretical formulation requires that the main stopping criterion in the above iterative formulation is to reach a target misfit value (to avoid fitting data to noise). However, in practice this has limited value since there is no objective way to get an accurate estimate of this misfit value, given that field data noise as estimated by instruments is only approximate and certainly unable to describe many other important sources of noise (i.e. modeling, linearization errors etc.). Thus we have adopted the observation of a slow convergence rate as a single stopping criterion, which is commonly used by many researchers (Loke and Barker, 1996a). In this case, the iterative procedure described in Eq. (5) ends when no significant improvement (i.e. 5%) of the RMS error is observed, where the RMS is given by:

$$\mathrm{RMS} = \sqrt{\sum_{i=1}^{n} \mathrm{d}y_i^2/\sigma_i^2 \Big/ \sum_{i=1}^{n} 1/\sigma_i^2} = \sqrt{S \Big/ \sum_{i=1}^{n} 1/\sigma_i^2}, \quad (4)$$

where S is given by Eq. (2a). Eq. (4) shows that minimization of RMS is equivalent to minimization of S in the case of independent data errors for the typical Bayesian formulation. In the case of constant or not available data errors Eq. (4) becomes the usual:

$$\mathrm{RMS} = \sqrt{\sum_{i=1}^{n} \mathrm{d}y_i^2 \Big/ \mathrm{n}}, \quad (5)$$

A 2.5D Finite Element Method (FEM) scheme was used as the platform for the forward resistivity calculations (Tsourlos et al., 1999). The scheme uses crossed triangular elements for the FEM grid while a sparser grid of rectangular inversion parameters is overlain over it, as shown in Fig. 1. The adjoint equation approach (McGillivray and Oldenburg, 1990) was incorporated into the FEM scheme in order to calculate the Jacobian matrix **J**, which is also transformed to be in line with the applied logarithmic data and model parameterization (Park and Van, 1991).

The described algorithm was used to the dipole–dipole and Wenner–Schlumberger synthetic data sets obtained using the measuring scheme described in the previous paragraph for the model of Fig. 2. The model consists of a rectangular prism with a high resistivity of 400 Ohm–m embedded in a medium with a lower resistivity of 100 Ohm–m, which overlies above another

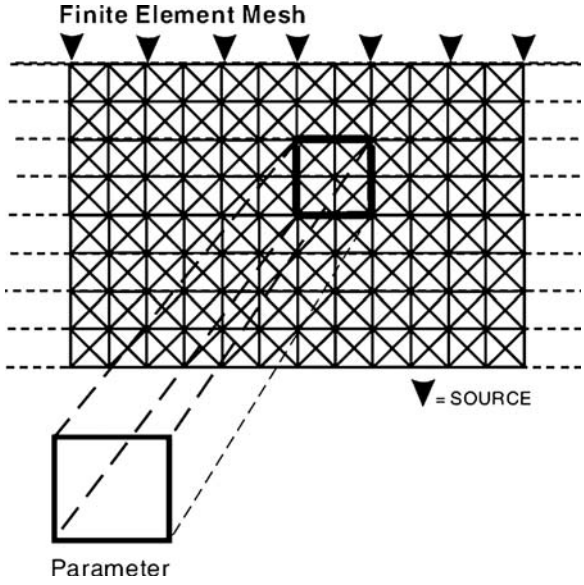

Fig. 1. FEM crossed triangular element mesh used in this work. Several elements are assembled to form a rectangular inversion parameter.

medium with a resistivity of 200 Ohm–m. Note that the borders of the modeling body do not coincide with the borders of the parameter grid. The apparent resistivity values of a multi-electrode configuration of 26 equally spaced electrodes with spacing "a" set to 5 m using the dipole–dipole and Wenner–Schlumberger arrays were calculated with a finite element scheme using a maximum n-separation $n_{\max}=8$a. Realistic random noise of 1 mV/A peak-to-peak amplitude was applied to the synthetic data (Yi et al., 2003).

The inversion results are presented in Fig. 3. The geoelectrical model obtained by the inversion of the dipole–dipole data set (Fig. 3b) clearly depicts the submerged body but the boundary between the two layers is not clearly identified. On the other hand, the geoelectrical model obtained by the inversion of the Wenner–Schlumberger data set (Fig. 3c) shows the boundary between the two layers but the submerged body is not reconstructed equally well.

In Fig. 3d the geoelectrical model obtained by the combined inversion of both dipole–dipole and Wenner–Schlumberger data sets is presented. It is quite evident that this inverted geoelectrical model is almost identical to the geoelectrical model obtained by the dipole–dipole data set. This happens because the measurements taken with the dipole–dipole array correspond to higher sensitivity values and subsequently have a higher contribution to the joint inversion than the measurements taken with the Wenner–Schlumberger array, hence the dipole–dipole data dominate the Wenner–Schlumberger data.

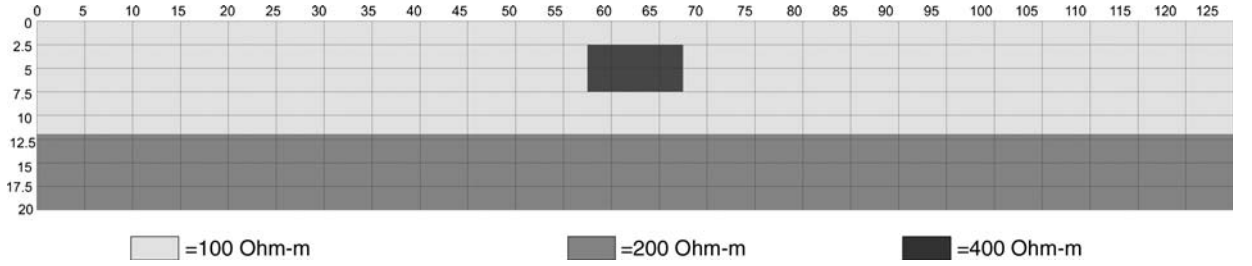

Fig. 2. The synthetic model employed to produce the dipole–dipole and Wenner–Schlumberger synthetic data.

Therefore, in order to produce a reliable geoelectrical inverted model of the subsurface by taking into account all available information, a combined weighted inversion algorithm needs to be considered. The existing algorithm has been modified by introducing an extra weighting factor, which attempts to balance out the contribution of the various resistivity array measurements into the inversion. If M is the total number of the observed data coming from different arrays, the weighting factor is introduced by means of an mxm diagonal matrix $\mathbf{W}_B$, and the ith element of which is defined as:

$$\mathbf{W}_{Bii} = \begin{cases} b_i = 1 & \text{if } i \text{ is a measurement of the reference array A} \\ b_i = b^{B,C\ldots} & \text{if } i \text{ is a measurement of any other array B, C}\ldots \end{cases} \quad (i = 1, 2, \ldots M), \tag{6}$$

The term b takes values between $(0,\infty)$ for each array. This weighting factor effectively operates in a way similar to the data (error) weighting diagonal matrix $\mathbf{W}_d$ of Eq. (2),

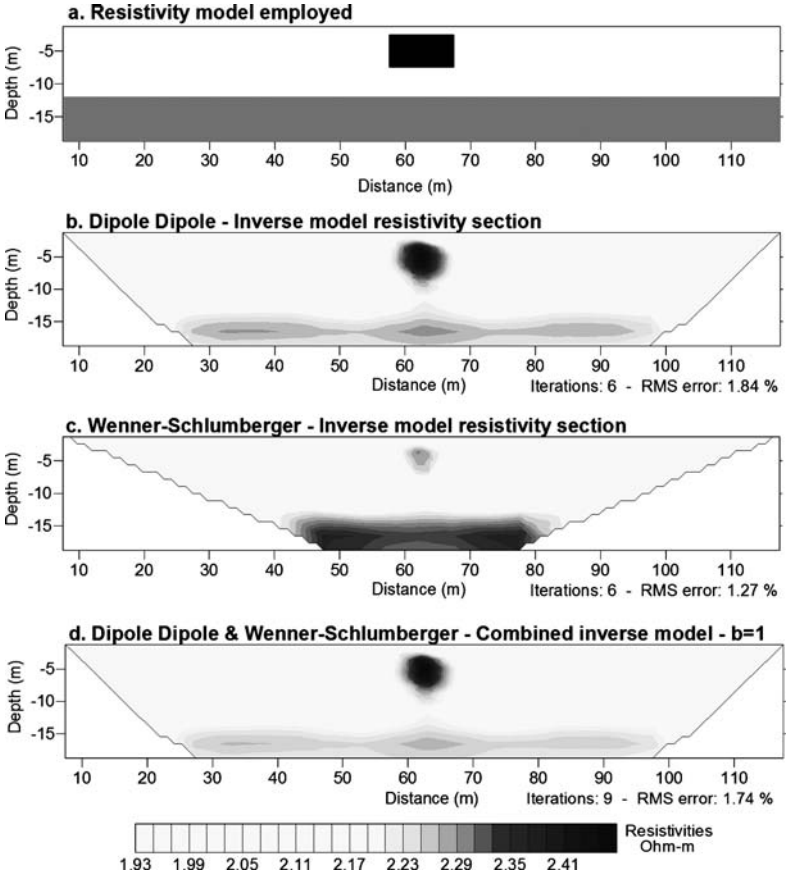

Fig. 3. Inversion results (1 mV/A added noise): (a) Resistivity model employed. (b) Dipole–dipole inverse model resistivity section. (c) Wenner–Schlumberger inverse model resistivity section. (d) Combined inverse model obtained by dipole–dipole and Wenner–Schlumberger data sets (no weighting).

i.e. the larger the value of b_i, the stronger the contribution of the measurements of array $\mathbf{W}_B$ in the inversion. The data misfit term S to be minimized (Eq. (2)) now becomes:

$$S = (\mathbf{W}_B\mathbf{W}_d\mathbf{dy})^T(\mathbf{W}_B\mathbf{W}_d\mathbf{dy}), \tag{7}$$

and the iterative inversion equation becomes:

$$\begin{aligned}\mathbf{x}_{k+1} &= \mathbf{x}_k + \mathbf{dx}_k = \mathbf{x}_k \\ &+ \left[(\mathbf{W}_B\mathbf{W}_d\mathbf{J}_k)^T(\mathbf{W}_B\mathbf{W}_d\mathbf{J}_k) + \mu_\kappa(\mathbf{C}_x^T\mathbf{C}_x + \mathbf{C}_z^T\mathbf{C}_z)\right]^{-1} \\ &\times(\mathbf{W}_B\mathbf{W}_d\mathbf{J}_k)^T(\mathbf{W}_B\mathbf{W}_d\mathbf{dy}_k),\end{aligned} \tag{8}$$

When b_i is 1 no additional weighting is effectively applied, while when it takes the value of 0 it is equivalent to excluding the measurements of the specific array from the inversion. On the other hand, high values of b_i are equivalent to minimizing the influence of the reference array A to the inversion.

Due to the differentiation of the objective function (Eqs. (2), (7)) the RMS misfit definition of Eq. (4) needs to be modified in order to accommodate the introduction of the weighting factor b_i. A weighted RMS misfit (RMS_w) can be defined by:

$$RMS_w = \sqrt{\sum_{i=1}^{M} b_i^2 dy_i^2/\sigma_i^2 \Big/ \sum_{i=1}^{M} b_i^2/\sigma_i^2}, \tag{9}$$

which in the case of constant or not available data errors becomes:

$$\begin{aligned}RMS_w &= \sqrt{\sum_{i=1}^{M} b_i^2 dy_i^2 \Big/ \sum_{i=1}^{M} b_i^2} \\ &= (RMS^A + b^B RMS^B + b^C RMS^C \\ &\quad + \ldots)/(1 + b^B + b^C + \ldots),\end{aligned} \tag{10}$$

Eqs. (7) and (9) describe in detail the way that the performed weighting works in practice: the data error, σ_i, is modified by the scaling factor, b, of each array. This is performed by considered an updated data error σ_i/b_i, which is either smaller or larger than the original one, depending on the specific scale factor of the array to which it belongs. This modification also affects the specific datum (and corresponding array) impact on the final solution. Moreover, Eq. (10) suggests that the final weighted RMS is a weighted average of the RMS of the individual arrays for the specific final model derived through the iterative procedure of Eq. (8).

3. Weighting factor calculation

In order to find the optimum value of the weighting factor b, which will enable the proportional contribution of all measurements in the inversion, four different approaches were examined (Athanasiou, 2004). Two of these methods were based on the Jacobian matrices $\mathbf{J}^A$ and $\mathbf{J}^B$ of the two arrays, A and B (Eq. (11)).

$$\mathbf{J}^A = \begin{pmatrix} J_{11}^A & J_{12}^A \ldots & J_{1M}^A \\ J_{21}^A & J_{22}^A \ldots & J_{2M}^A \\ \vdots & \vdots & \vdots \\ J_{N1}^A & J_{N2}^A \ldots & J_{NM}^A \end{pmatrix} \quad \text{and}$$

$$\mathbf{J}^B = \begin{pmatrix} J_{11}^B & J_{12}^B \ldots & J_{1M}^B \\ J_{21}^B & J_{22}^B \ldots & J_{2M}^B \\ \vdots & \vdots & \vdots \\ J_{N1}^B & J_{N2}^B \ldots & J_{NM}^B \end{pmatrix}, \tag{11}$$

According to the first method which employs the Jacobian matrices, the weighting factor b is estimated by the equations:

$$J_j^A = \frac{\sum_{i=1}^{N_A} |J_{ij}^A|}{N_A} \quad , \quad J_j^B = \frac{\sum_{i=1}^{N_B} |J_{ij}^B|}{N_B} \quad \text{and} \tag{12}$$

$$b = \sum_{j=1}^{M} \frac{J_j^A}{J_j^B} \quad (j = 1, 2, \ldots M),$$

where J_{ij}^A are the elements of the reference array A Jacobian matrix $\mathbf{J}^A$, J_{ij}^B are the elements of the array B Jacobian matrix $\mathbf{J}^B$, J_j^A are the means of the absolute values of J_{ij}^A for every parameter of the reference array A and J_j^B are the means of the absolute values of J_{ij}^B for every parameter of the array B. The weighting factor b is given by the sum of the ratios between J_j^A and J_j^B and is a constant scalar quantity for all measurements of array B. Since the Jacobian matrices are updated in every iteration, b is also recalculated. However, the difference of the new weighting factor in relation to the weighting factor of the previous iteration is very small (<1%).

According to the second method, the weighting factor b for the Jacobian matrices $\mathbf{J}^A$ and $\mathbf{J}^B$ (Eq. (11)) is estimated by the equations:

$$J_j^A = \frac{\sqrt{\sum_{i=1}^{N_A} |J_{ij}^A|^2}}{N_A} \quad , \quad J_j^B = \frac{\sqrt{\sum_{i=1}^{N_B} |J_{ij}^B|^2}}{N_B} \quad \text{and}$$

$$b = \sum_{j=1}^{M} \frac{J_j^A}{J_j^B}, \tag{13}$$

Eqs. (12) and (13) are equivalent to calculating the mean L_1 and L_2 column norms of the Jacobian matrices of the two arrays.

A reasonable alternative to the use of Jacobian matrices, in order to define the weighting factor b of each array, is to use the ratio of the L_2 and L_1 column norms of the measured resistivities (data vectors). In these two cases, the sensitivity of each array is determined directly by the data and not by the data-model derivatives. This approach has been also tested in the present work.

The variation of the weighting factor values, which are calculated by the four methods is usually fluctuating over a very small range of values, of the order of a few percent. This observation suggests that these methods are quite appropriate for the definition of b since the data which are used (data resistivities or Jacobian matrices) are directly depended and express the relative sensitivity of one array

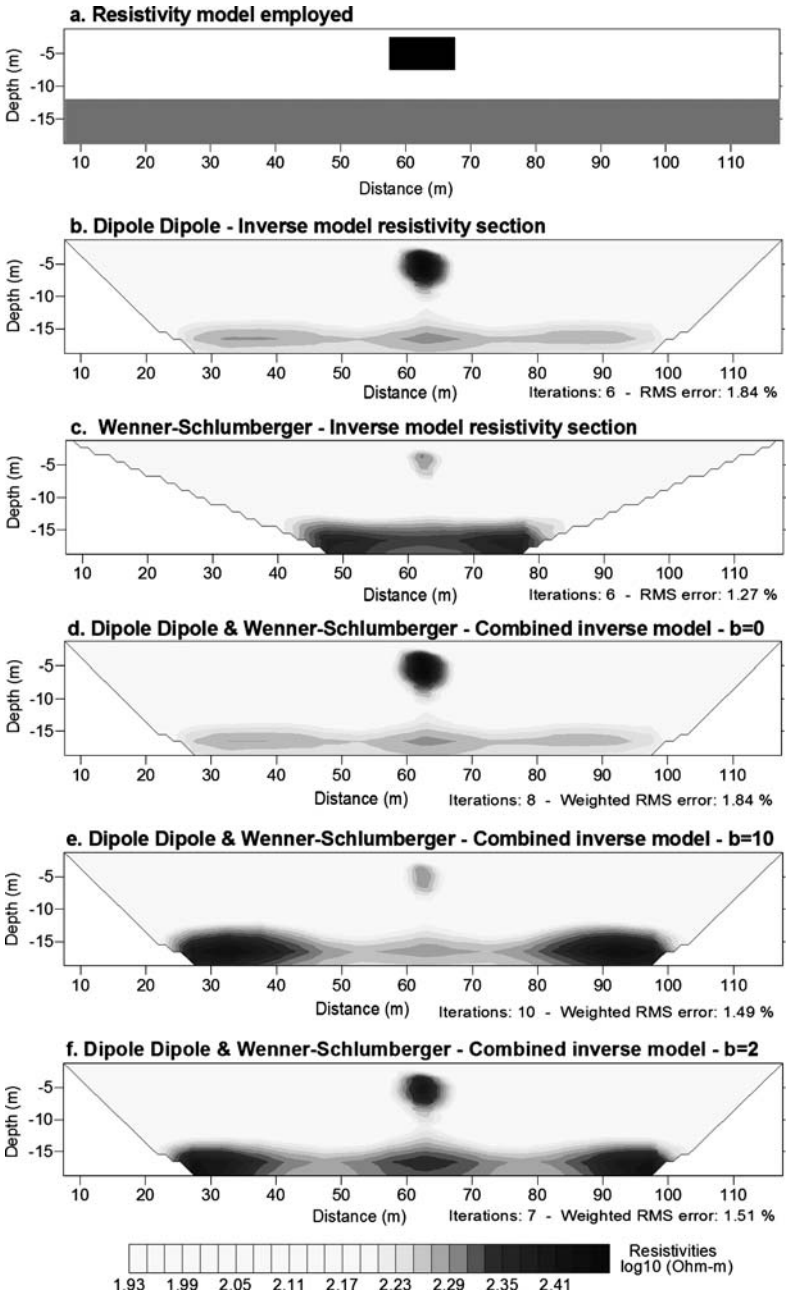

Fig. 4. Inversion results (1 mV/A added noise): a) Resistivity model employed. (b) Inverse model obtained by dipole–dipole data set. (c) Inverse model obtained by Wenner–Schlumberger data set. (d), (e) and (f) Combined inverse models obtained by dipole–dipole and Wenner–Schlumberger data sets for three different values of the weighting factor.

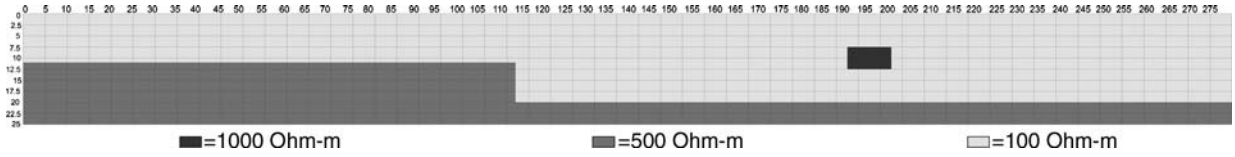

Fig. 5. The first synthetic model employed to produce the dipole–dipole and Wenner synthetic data.

to another. Furthermore, after taking into account a large number of trials, we observed that the value of the weighting factor b is almost constant for each array combination, independently of the specific model used.

In this work we have chosen the weighting factor b which was calculated with the second method based on the Jacobian matrices (Eq. (13)), since it appeared that in every examined case it represented the median value of the weighting factors calculated by all four methods.

In Fig. 4 the geoelectrical models obtained by the combined weighted inversion of dipole–dipole and Wenner–Schlumberger data set for three different values

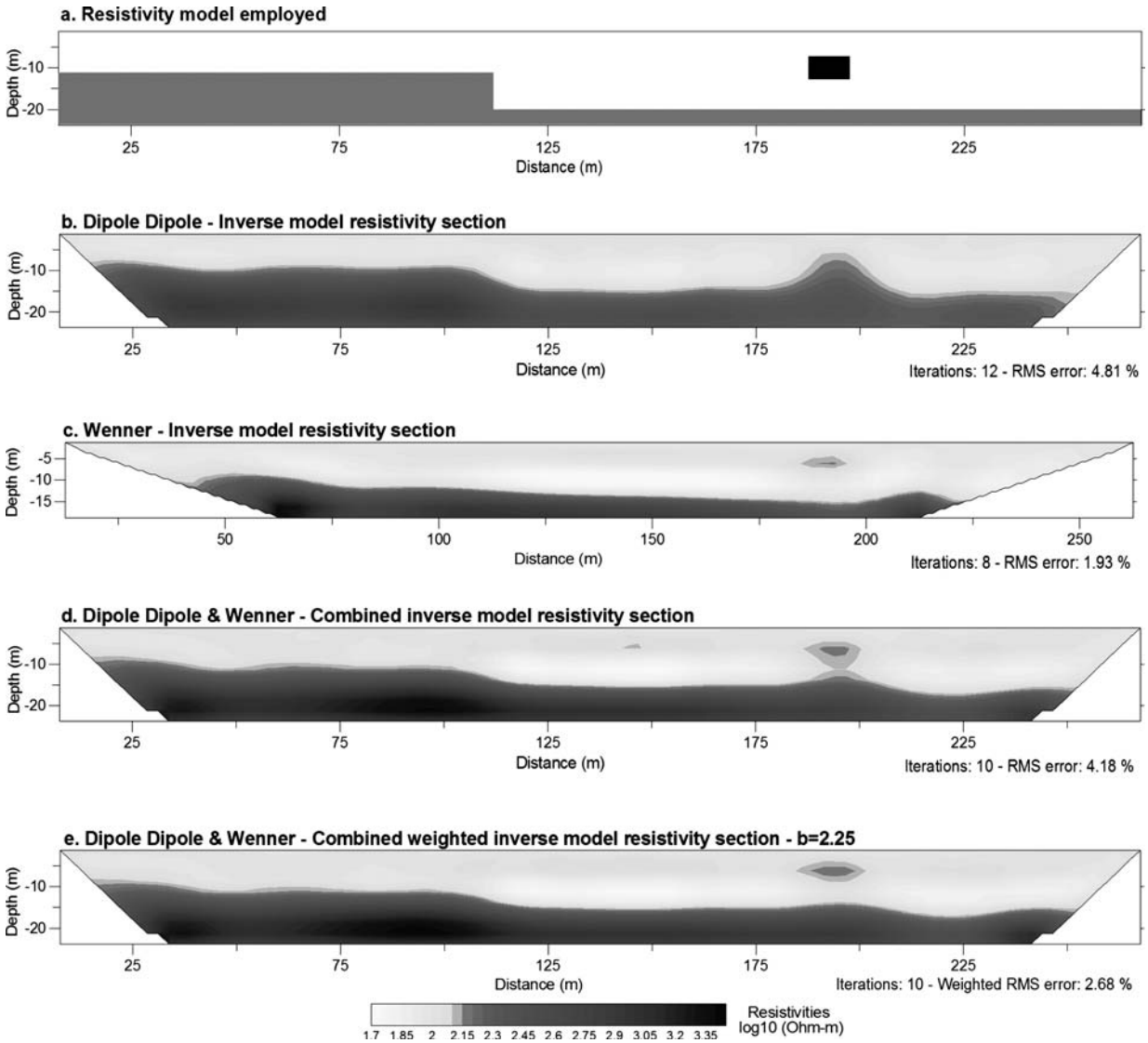

Fig. 6. Inversion results (3 mV/A added noise): (a) Resistivity model employed. (b) Inverse model obtained by dipole–dipole data set. (c) Inverse model obtained by Wenner data set. (d) Combined inverse model obtained by dipole–dipole and Wenner data sets. (e) Combined weighted inverse model obtained by dipole–dipole and Wenner data sets using the weighting scheme proposed in the present work ($b=2.25$).

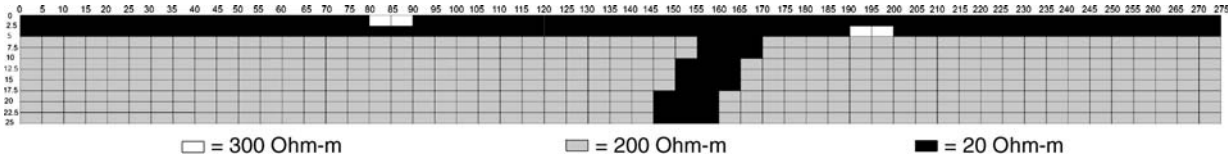

Fig. 7. The second model used to produce the dipole–dipole, pole–dipole and Wenner synthetic data.

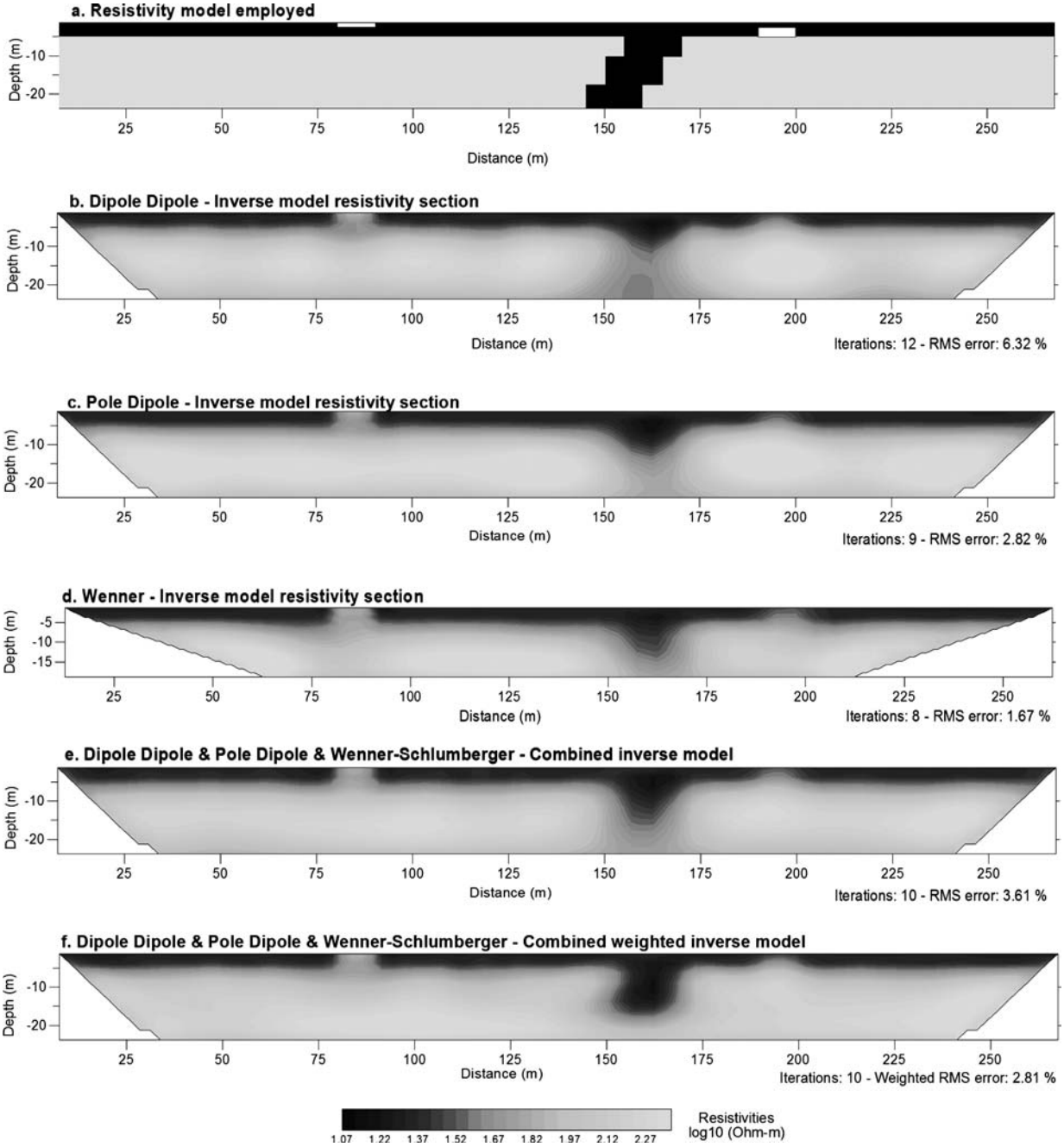

Fig. 8. Inversion results (3 mV/A added noise): (a) Resistivity model employed. (b), (c) and (d) Inverse models obtained by dipole–dipole, pole–dipole and Wenner data sets respectively. (e) Combined inverse model obtained by dipole–dipole, pole–dipole and Wenner data sets. (f) Combined weighted inverse model obtained by dipole–dipole, pole–dipole and Wenner data sets.

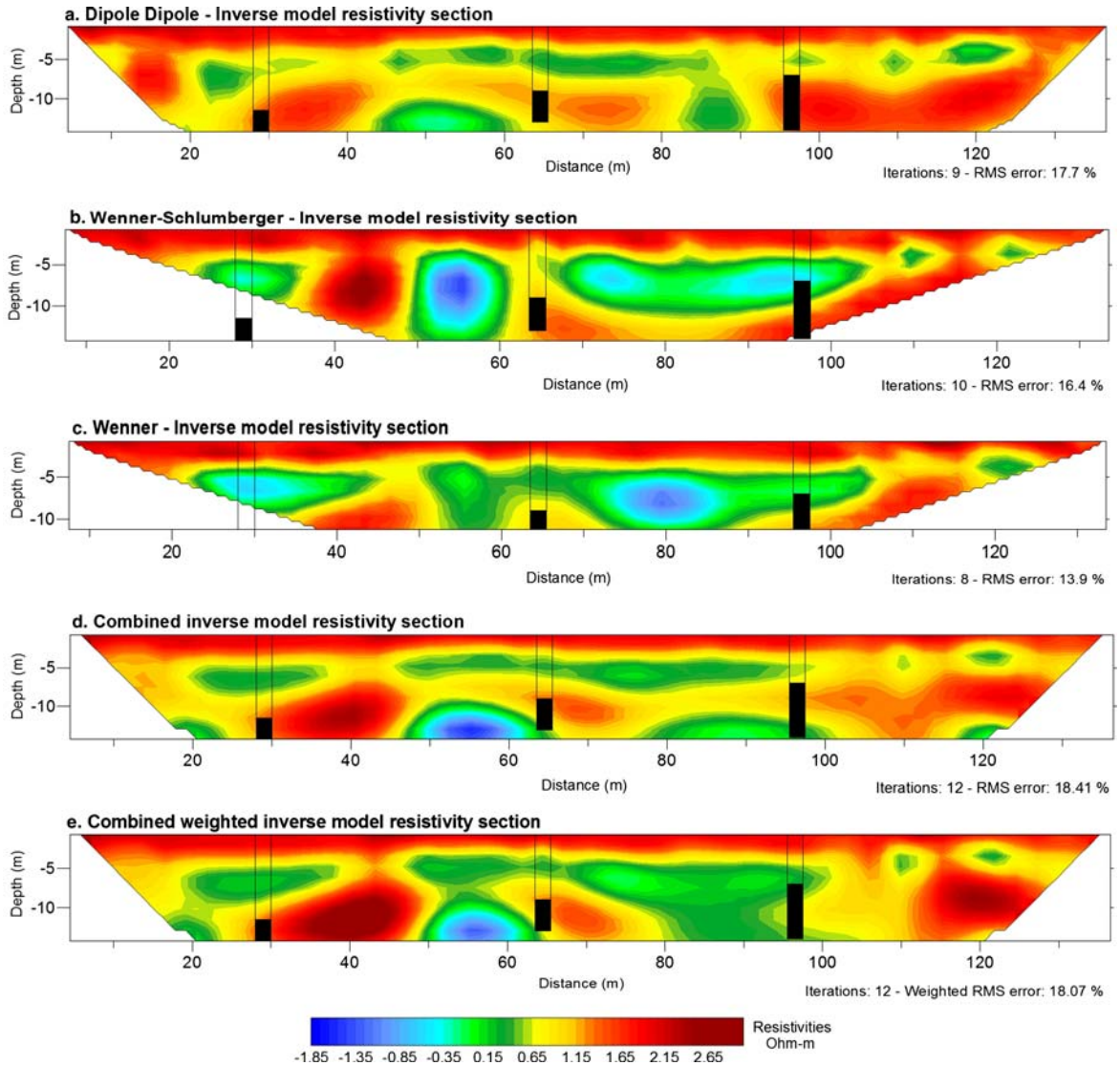

Fig. 9. Inversion results: (a), (b) and (c) Inverse model resistivity sections obtained by dipole–dipole, Wenner–Schlumberger and Wenner data sets respectively. (d) Combined inverse model obtained by dipole–dipole, Wenner–Schlumberger and Wenner data sets with no weight. (e) Combined inverse model obtained by dipole–dipole, Wenner–Schlumberger and Wenner data sets with optimum weight.

of b are presented. When $b=0$ the sensitivity of the array B measurements is zero and this is equivalent to excluding these measurements from the inversion. This is indicated in Fig. 4d, which shows the combined inversion of the two data sets with a weighting factor $b=0$. The inverted geoelectrical model is practically identical to the model produced by the inversion of the dipole–dipole data set (Fig. 4b).

By assigning a large value of b (e.g. $b=10$) the sensitivity of the array B measurements is reinforced, which is equivalent to minimizing the influence of the reference array A measurements on the inversion. This is indicated in Fig. 4e, which shows the combined inversion of the two data sets with a weighting factor $b=10$. The inverted geoelectrical model is similar to the model produced only by the inversion of the Wenner–Schlumberger data set (Fig. 4c).

Finally, in Fig. 4f the inverted geoelectrical model produced by the combined inversion of the two data sets with a weighting factor $b=2$ is presented. This value is estimated by the adopted method based on the Jacobian matrices, as it is described above (Eq. (13)). The deduced geoelectrical model combines the characteristics of both the dipole–dipole and Wenner–Schlumberger geoelectrical models and reconstructs the initial model more effectively.

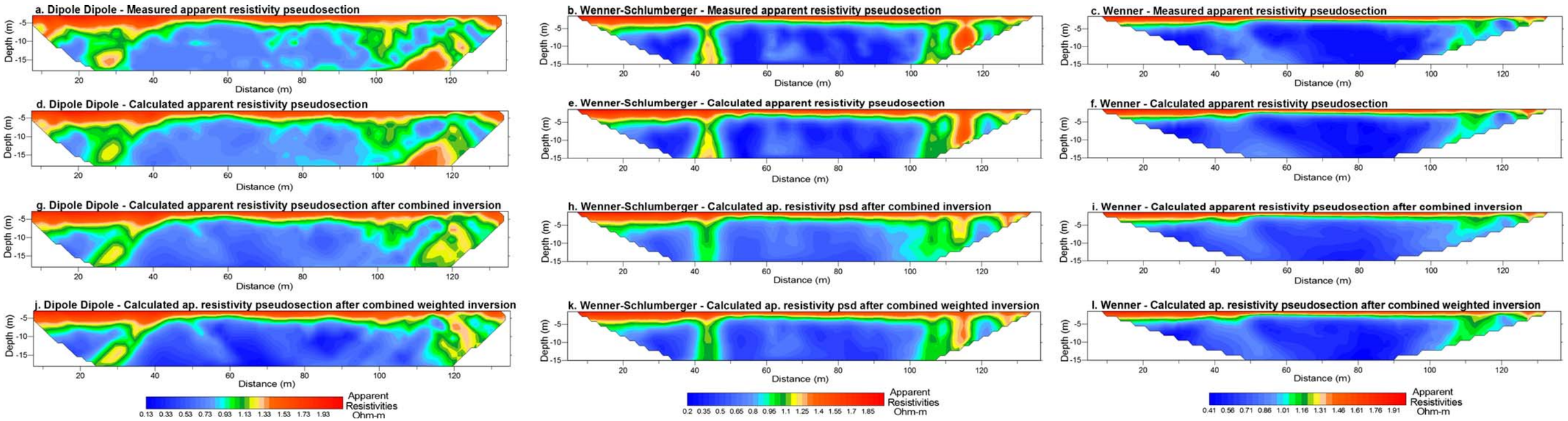

Fig. 10. Pseudosections: (a), (b) and (c) Dipole–dipole, Wenner–Schlumberger and Wenner measured ap. resistivity pseudosections. (d), (e) and (f) Dipole–dipole, Wenner–Schlumberger and Wenner calculated ap. resistivity pseudosections. (g), (h) and (i) Dipole–dipole, Wenner–Schlumberger and Wenner calculated ap. resistivity pseudosections obtained by combined inversion. (j), (k) and (l) Dipole–dipole, Wenner–Schlumberger and Wenner calculated ap. resistivity pseudosections obtained by combined weighted inversion.

4. Application of the algorithm to synthetic data

The described algorithm was applied to a series of synthetic models. In this section the results from tests conducted using two synthetic data sets are given. The first model (Fig. 5) consists of a sharp contact between media of highly different resistivity (500 Ohm–m and 100 Ohm–m). On the right, a rectangular resistive body is embedded in the more conductive medium of the two media. The apparent resistivity values of a multi-electrode configuration of 56 equally spaced electrodes using spacing "a" set to 5 m using the dipole–dipole and Wenner arrays were calculated with a finite element scheme with a maximum n-separation $n_{max}=8a$. Random noise of 3 mV/A peak-to-peak amplitude was applied to the synthetic data.

The inversion results are presented in Fig. 6. It is seen that the geoelectrical model obtained by the inversion of the dipole–dipole data set (Fig. 6b) clearly delineates the contact between the two media, but the submerged body is not distinguished from the underlying layer. In the geoelectrical model obtained by the inversion of the Wenner data set (Fig. 6c) the two layers are shown but not the abrupt contact between them. Furthermore, the submerged body is only slightly indicated.

The combined un-weighted inverse geoelectrical model obtained by both dipole–dipole and Wenner data sets is presented in Fig. 6d. In this model the contact between the two media is delineated but not as clear as in the dipole–dipole inverse model. On the other hand, the submerged body is better identified in comparison with the image taken from the dipole–dipole and Wenner inverse models but still appears "connected" to the underlying layer, resembling more the dipole–dipole inversion results.

In Fig. 6e the geoelectrical model obtained by the combined weighted inversion of both the dipole–dipole and Wenner data sets is presented. It is observed that this model delineates the contact between the two media and further, the submerged body is clearly indicated and separated from the underlying layer.

The second model (Fig. 7) has a more complicated structure. First, a medium with a resistivity of 20 Ohm–m overlies a medium with a resistivity of 120 Ohm–m. On the left, one resistive body (300 Ohm–m) is situated into the first conductive layer (20 Ohm–m). On the right, a slightly dipping conductive "fractured" zone with a resistivity of 20 Ohm–m is cutting across the layer of 120 Ohm–m, whereas a resistive body of 300 Ohm–m is submerged in to the first conductive layer. The apparent resistivity values of a multi-electrode configuration of 56 equally spaced electrodes with spacing "a" set to 5 m using the dipole–dipole, pole–dipole and Wenner arrays were calculated with a finite element scheme using a maximum n-separation $n_{max}=8a$. Random noise of 3 mV/A peak-to-peak amplitude was applied to the synthetic data.

The inverted models are presented in Fig. 8. As it is observed all the geoelectrical inverted models show the position of the fractured zone and the two shallow buried bodies. The dipole–dipole array type shows quite well the full vertical extent of the fractured zone but gives no information about its dip (Fig. 8b). The pole–dipole array type does not show neither the extent of the fault zone nor its dip (Fig. 8c). The Wenner array shows the fault zone in a satisfactory extent but with a slight dip to the wrong direction (Fig. 8d).

The combined un-weighted inverted model (Fig. 8e) shows the fractured zone in a satisfactory extent and the position of the two shallow buried bodies. As it is seen, this model is quite similar to the results of the dipole–dipole array which, due to its higher sensitivity, "dominates" the inversion image. The combined weighted inverted model, shown in Fig. 8f, depicts the fractured zone and the two shallow buried bodies satisfactorily. Although different, it is difficult to say which of the two combined inversions (weighted or un-weighted) reconstructs the model better. It has to be noted that in this case the combined inversion result (weighted or not) does not yield a better result than an individual array inversion (viz. dipole–dipole). Yet given that usually interpreter, due to limited prior information, is unable to judge which independent array result is better, the combined data sets inversion can produce a sensible fusion of all available information into a single representative image.

5. Application of the algorithm to real data

The application of the algorithm to synthetic data produced satisfactory results but it is obvious that, as far as this algorithm is designed for field data interpretation, it must be tested with real data in order to deduce convincing results. Furthermore, these real data should be taken from a known target in order to verify the inversion results. The data set on which the combined weighted inversion algorithm was applied was obtained over a sidewalk situated next to the Faculty of Sciences building of the Aristotle University of Thessaloniki (Greece). Note that the above experiment has been conducted in an environment complicated by anthropogenic features (pavement, metal pipes etc.) with expected high levels of noise and apparently 3-D effects. Despite the noisy environment the measurements themselves exhibited a low standard deviation, routinely below 5%.

The aim of this survey was the study of the subsurface geoelectrical structure and especially the location of the basement, which outcrops a few meters northwards from the studying area and underlies recent sediments along of the electrical survey line. The basement comprises mainly from green gneisses, which are representative of the region of Thessaloniki. The surface formations consist of a rabble cover in the first few meters and thereafter alluvial deposits and deposits which come from the erosion of the basement.

Dipole–dipole, Wenner–Schlumberger and Wenner arrays were measured over the survey area. The measured section involved 48 electrodes, with "a" spacing equal to $a=3$ m and the maximum n-separation was $n_{max}=7$ for electrode spacings "a" and "$2a$". The geoelectrical inverted models of individual arrays are depicted in Fig. 9a–c and the corresponding field and model data pseudosections are shown in Fig. 10a–c and Fig. 10d–f respectively.

Information was also available from three boreholes, which were drilled lengthways of the section. Black frames in the inverted sections of Fig. 9 are used to depict the position of the boreholes in the geoelectrical inverted models, while the basement (gneiss) as recorded by the boreholes is shown with black color.

It is observed that the geoelectrical models deduced by all arrays exhibit some differences. Despite their differences the results are in general, but not in full, agreement with the information taken by the drills, as far as the depth of the basement is concerned. In all geoelectrical models of Fig. 9 the low-resistivity formations are presented with cold colors, whereas the high-resistivity formations (such as the basement) are presented with warm colors. The high values of resistivity in very small depths indicate the existence of the rabble due to anthropogenic activity. According to this information, the upper surface of the basement is recorded at the depth of 11.5 m at the beginning of the section as shown by the first drill and thereafter it rises to 9 m and finally at 7 m as shown by the last drill.

The joint inversion of data from all arrays would be considered as a reasonable step to produce a more informative subsurface image. The combined inverted model produced by all measured arrays without any weighting is shown in Fig. 9d and it is quite clear that it is closer to the results of the dipole–dipole array which, due to its higher sensitivity, "dominates" the inversion image. This is also manifested in Fig. 10g–i in which the calculated data pseudosections of the arrays participating into the un-weighted inversion are plotted: the dipole–dipole calculated data pseudosection (Fig. 10g) is quite close to the corresponding field data (Fig. 10a), while this is not the case for the other two arrays (Fig. 10g–i).

Conversely, the results of the combined weighted inversion are depicted in Fig. 9e, showing a different image which is a more representative mixture of the independent inversion images. The corresponding calculated data pseudosections of the Wenner–Schlumberger and Wenner arrays (Fig. 10k–l) are in better agreement with the filed data than in the un-weighted inversion case, but as expected, this is not the case for the calculated dipole–dipole data (Fig. 10j).

The RMS errors of the combined and combined weighted inverted models are slightly larger than those of the individual inverted models due to the attempt of the algorithm to combine information of different array types.

6. Discussion and conclusions

In this work the case of 2-D combined inversion of resistivity data arising from different array types is examined. Simple structures are adequately described from all array types as well as from their combination. However, as the structures become more complicated the information taken from each array individually becomes increasingly diverse. This approach can provide improved subsurface images as it jointly inverts arrays with different characteristics. For example, it combines Wenner and Wenner–Schlumberger arrays, which have high vertical resolution with dipole–dipole and pole–dipole arrays, which have high lateral resolution. The main disadvantage of the method, which is the extra time to acquire a large number of measurements, is partly compensated by the increased measuring speed of automated resistivity meters.

It is shown that some arrays dominate over others during the joint inversion procedure and therefore the un-weighted combined inversion geoelectrical model is more similar to the geoelectrical model produced by the dominant array. The scheme described in the present work includes a weighting factor which partly balances the participation of the arrays. The use of combined weighted inversion requires the introduction of an extra factor, which needs to be calculated during inversion. However, this factor is calculated automatically in a fairly simple manner and is easily incorporated in the algorithm so that no extra processing is needed.

From the study of the several test models it can be deduced that the weighting factor "b" depends on the number and the geometry of the electrodes used, whereas is independent of the distribution of the measured resistivities. Thereby, for a particular array combination, in which a specific number of electrodes are used, the weighting factor "b" is practically independent of the initial model.

It could be argued that there is no need to introduce such an "array correction" factor and that the original misfit definition incorporates in the Bayesian sense the data errors, σ_i, which are used in the misfit function (2) and the corresponding RMS (Eq. (4)). However, in practice, estimates of data-point errors are not always available and if available not always reliable e.g. data-points with small standard deviations are obvious outliers and vise-versa. Furthermore, the actual errors that should be included in Eq. (2) are a combination of both the observation errors, as well as of the modeling errors due to poor modeling (2-D models of a 3-D earth, anisotropy, limitations of forward modeling, fixed parameter boundaries etc.) and the non-linearity (solution of a linearized scheme) of the inverse problem. This can be demonstrated in a simplified manner if we consider that any solution, $d\mathbf{x}_k$, of a linearized inverse problem is obtained by applying a linear operator, $\mathbf{L}$, on the observed data residuals, $d\mathbf{y}^{obs}$, as for example is seen in Eqs. (3) and (8). Therefore, we can write the following equation:

$$\begin{aligned} d\mathbf{x}_k &= \mathbf{L}d\mathbf{y}^{obs} = \mathbf{L}(d\mathbf{y}^{true} + \boldsymbol{\varepsilon}^{obs}) \\ &= \mathbf{L}\mathbf{J}d\mathbf{x}^{true} + \mathbf{L}\boldsymbol{\varepsilon}^{Lin-Mod} + \mathbf{L}\boldsymbol{\varepsilon}^{obs} \end{aligned} \quad (14)$$

where $\boldsymbol{\varepsilon}^{obs}$ is the observed (measurement) data error vector and $\boldsymbol{\varepsilon}^{Lin\text{-}Mod}$ corresponds to the combined modeling/linearization error vector.

Eq. (14) shows that our solution suffers not only because of observational errors but also due to errors introduced by linearization and modeling simplifications, as well as by errors introduced due to the specific choice of $\mathbf{L}$ which allows us to obtain a robust solution (e.g. for non-unique problems) at the cost of limited model resolution (typically described by the model resolution matrix $\mathbf{LJ}$). In practice the first two terms in Eq. (14) and especially the modeling-linearization errors are often much larger than the observational errors. It is clear that such modeling errors are not of the same scale for every electrode array but are actually scaled differently on the basis of the different sensitivities that the individual arrays exhibit, as this is expressed by the respective Jacobian matrices. Therefore, the largest part of the misfit function, S, or the equivalent RMS expressions which are minimized are controlled by sensitivity-dependent errors, which may have nothing to do with the actual observational errors (that are often only implicitly estimated). For this reason, the selected weighted factors used in the proposed scheme are calculated as expressions of the arrays' Jacobian matrices (see Eqs. (12) and (13) for b_i estimation), reflecting in this way the variable sensitivity of the different electrode arrays. Note that the proposed formulation not only allows for the incorporation of modeling sensitivity errors through b_i (matrix $\mathbf{W}_B$) but still allows for the incorporation (Eq. (7)) of individual data observation errors, if available (matrix $\mathbf{W}_d$).

Results, presented in this work indicate that the combined weighted inversion produces a fused geoelectrical model which is more representative of the study area compared to the one produced by just jointly inverting all data sets without weighting. It has to be stressed though that, as suggested by the examples presented in this work, there is absolutely no guarantee that the combined inversion (weighted or not) results of geoelectrical data from different arrays will produce subsurface images which are superior to the ones produced by individual array inversions. To the contrary, in the case that an individual array inversion is more representative of reality any combined inversion result will be at best equal or inferior. Similarly, inclusion of a low quality data set into the joined inversion scheme would probably produce results inferior to the inversions of individual (higher quality) array data sets. In this framework a further use of the proposed weighting scheme can be suggested: depending on the quality of the individual array inversion results (e.g. on the basis of the correlation with prior information) the user could increase or decrease the weighting factor b_i of a particular array, at an arbitrary level, to increase or decrease its contribution into the final inversion result. Admittedly, this has a high degree of subjectivity and is not necessarily a good filed practice.

Overall, the usefulness of the combined weighted inversion algorithm consists in the combination of data of various array types, especially when the arrays cannot separately produce a reliable geoelectrical model in case of complicated subsurface structure under no or limited prior information.

Acknowledgements

This work is supported by the EU project: "Sustainable management of water resources by automated real-time monitoring (ALERT)", contract No GOCE-CT-2004-505329. The authors would like to thank Dr. Jun-Ho Kim, the editor Dr. Hordt and two anonymous reviewers for their very useful suggestions and constructive criticism.

References

Athanasiou, E., 2004. Combined inversion of geoelectrical data by the use of contact electrodes. M.Sc. Thesis, Aristotle University of Thessaloniki.

Dahlin, T., 2001. The development of DC resistivity imaging techniques. Computers & Geoscience 27 (9), 1019–1029.

Dahlin, T., Zhou, B., 2004. A numerical comparison of 2D resistivity imaging with 10 electrode arrays. Geophysical Prospecting 52, 379–398.

de Groot-Hedlin, C., Constable, S., 1990. Occam's inversion to generate smooth, two-dimensional models from magnetoteluric data. Geophysics 55, 1613–1624.

de la Vega, M., Osella, A., Lascano, E., 2003. Joint inversion of Wenner and dipole–dipole data to study a gasoline-contaminated soil. Journal of Applied Geophysics 54, 97–109.

Griffiths, D., Barker, R., 1993. Two dimensional resistivity imaging and modeling in areas of complex geology. Journal of Applied Geophysics 19, 211–226.

LaBrecque, D., Miletto, M., Daily, W., Ramirez, A., Owen, E., 1996. The effects of noise on "Occam" inversion of resistivity tomography data. Geophysics 61, 538–548.

Li, Y., Oldenburg, W., 1992. Approximate inverse mapping in DC resistivity problems. Geophysical Journal International 109, 343–362.

Loke, M.H., Barker, R., 1995. Least-squares deconvolution of apparent resistivity pseudosections. Geophysics 60, 1682–1690.

Loke, M.H., Barker, R., 1996a. Rapid least-squares inversion of apparent resistivity pseudosections by a quasi-Newton method. Geophysical Prospecting 44, 131–152.

Loke, M.H., Barker, R., 1996b. Practical techniques for 3D resistivity surveys and data inversion. Geophysical Prospecting 44, 499–523.

McGillivray, P., Oldenburg, D., 1990. Methods for calculating Frechet derivatives and sensitivities for the non-linear inverse problem. A comparative study. Geophysical Prospecting 38, 499–524.

Park, S.K., Van, G.P., 1991. Inversion of pole–pole data for 3-D resistivity structure beneath arrays of electrodes. Geophysics 56, 951–960.

Sasaki, Y., 1992. Resolution of resistivity tomography inferred from numerical simulation. Geophysical Prospecting 40, 453–464.

Stummer, P., Maurer, H., Green, A., 2004. Experimental design. Electrical resistivity data sets that provide optimum subsurface information. Geophysics 69 (1), 120–139.

Tarantola, A., 1984. Inversion of seismic reflection data in the acoustic approximation. Geophysics 49 (8), 1259–1266.

Tsourlos, P., 1995. Modelling interpretation and inversion of multi-electrode resistivity survey data. Ph.D. Thesis, University of York.

Tsourlos, P.I., Szymanski, J.E., Tsokas, G.N., 1999. The effect of terrain topography on commonly used resistivity arrays. Geophysics 64 (5), 1357–1363.

Ward, S., 1989. Resistivity and induced polarization methods: in investigations in geophysics no 5. In: Ward, S. (Ed.), Geotechnical and Environmental Geophysics, vol. I. SEG, Tulsa, pp. 147–189.

Yi, M.J., Kim, J.H., Chung, S.H., 2003. Enhancing the resolving power of least-squares inversion with active constraint balancing. Geophysics 68 (3), 931–941.